

Contents lists available at [SciVerse ScienceDirect](http://www.sciencedirect.com)

Biomaterials

journal homepage: www.elsevier.com/locate/biomaterials

Leading opinion

The use of nanoparticulate delivery systems in metronomic chemotherapy

De-Hong Yu^a, Fu-Qiang Ban^b, Mei Zhao^c, Qin Lu^a, Jonathan F. Lovell^d, Fan Bai^a, Chao Wang^a, Ying-Yun Guan^a, Xin Luan^a, Ya-Rong Liu^a, Chao Fang^{a,*}, Hong-Zhuan Chen^{a,*}^a Department of Pharmacology, Institute of Medical Sciences, Shanghai Jiao Tong University School of Medicine, 280 South Chongqing Road, Shanghai 200025, China^b Vancouver Prostate Center, University of British Columbia, 2660 Oak Street, Vancouver, BC V6H 3Z6, Canada^c Department of Pharmacy, Shanghai Institute of Health Sciences and Health School Attached to Shanghai Jiao Tong University School of Medicine, 279 Zhouzhu Road, Shanghai 201318, China^d Department of Biomedical Engineering, University at Buffalo, State University of New York, Buffalo, NY 14260, USA

ARTICLE INFO

Article history:

Received 21 January 2013

Accepted 7 February 2013

Available online xxx

Keywords:

Nanoparticles

Metronomic chemotherapy

Tumor angiogenesis

Docetaxel

Flt-1

SP5.2

ABSTRACT

Metronomic chemotherapy aiming at inhibiting tumor angiogenesis with conventional chemotherapeutics is a promising strategy for antiangiogenic cancer therapy. However, current metronomic chemotherapy mainly focuses on free small-molecule drugs, without any effort to achieve tumor-specific biodistribution, which may lead to long-term toxicity concerns. Metronomic chemotherapy using nanoparticulate drug delivery system (DDS) offers significant upside to reduce off-target side effects, decrease accumulated dose, and enhance the efficacy of tumor vessel targeting without compromising antitumor efficacy; but there has been a lack of thorough experimental data describing the targeted metronomic chemotherapy. Here, we develop a new nanoparticulate DDS, SP5.2 peptide conjugated, Flt-1 (VEGFR-1) targeted nanoparticles for docetaxel (SP5.2-DTX-NP), as a model for the investigation of targeted metronomic chemotherapy with respect to both antitumor efficacy and toxicity. The results demonstrate that metronomic SP5.2-DTX-NP exerts antitumor activity mainly through the antiangiogenic effect of docetaxel, which is specifically delivered into the tumor vascular endothelial cells through the nanoparticle internalization mediated by the interaction of SP5.2 and over-expressed Flt-1 receptors on tumor vessels. Moreover, the antitumor efficacy of targeted metronomic chemotherapy is better than that of the treatment with the DDS given in the maximum tolerated dose (MTD) regimen, which is shown in significantly prolonged mice survival and minimal drug-associated toxicity (bone marrow suppression, hematological toxicity, and mucosal injury of small intestine). The present research reveals and highlights the significance of targeted metronomic therapy with nanoparticulate DDS in antiangiogenic cancer therapy.

© 2013 Published by Elsevier Ltd.

1. Introduction

Tumor angiogenesis is a major therapeutic target in cancer therapy [1–5]. Six antiangiogenic drugs (Avastin, Nexavar, Votrient, Sutent, Caprelsa, and Inlyta) have been approved by FDA for various cancer indications. Besides these drugs, metronomic chemotherapy aiming at inhibiting tumor angiogenesis with conventional chemotherapeutics is emerging as a promising strategy for antiangiogenic cancer therapy in both preclinical studies and human clinical trials [6,7]. Metronomic chemotherapy is characterized by the frequent, even daily, administration of conventional

chemotherapeutics at doses significantly below the maximum tolerated dose (MTD) with no prolonged drug-free breaks. In contrast, MTD chemotherapy, as a mainstay in cancer treatment for decades, involves administration of a single dose or short courses of therapy at the highest doses possible without causing life-threatening toxicity.

The principal pharmacological basis of metronomic chemotherapy is that activated tumor vascular endothelial cells (EC) are more sensitive to low doses of chemotherapeutic drugs than the normal or parenchymal cancer cells when exposed in a frequent or continuous manner. Metronomic chemotherapy can also suppress the mobilization of circulating endothelial progenitors (CEPs) and induce the production of antiangiogenic glycoprotein thrombospondin 1 (TSP-1), an endogenous inhibitor, to reduce tumor neovascularization [6,7]. In addition, metronomic chemotherapy reduces time between dosing cycles, which may otherwise permit

* Corresponding authors. Tel./fax: +86 21 64674721.

E-mail addresses: fangchao100@hotmail.com (C. Fang), hongzhuan_chen@hotmail.com (H.-Z. Chen).

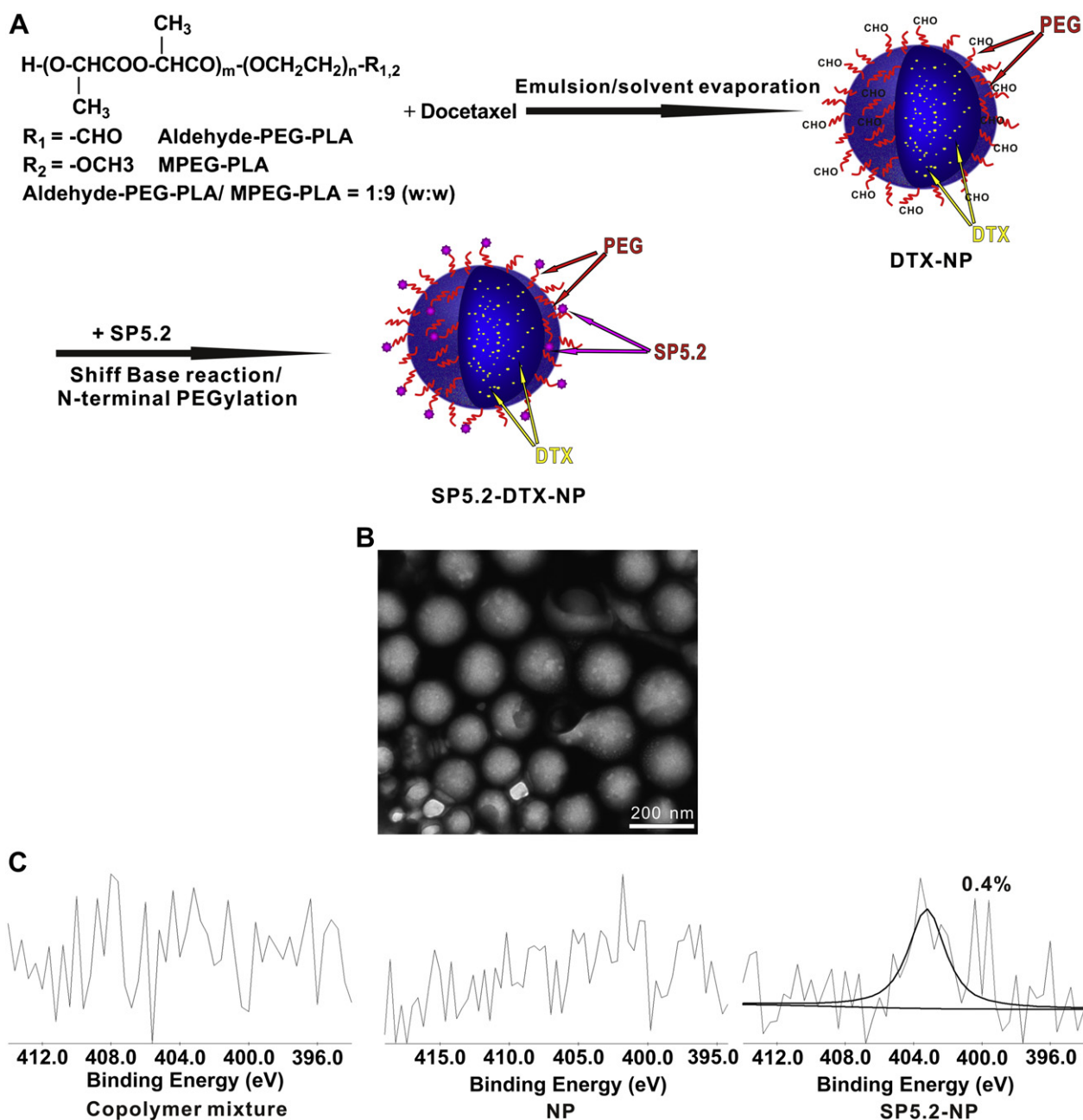


Fig. 1. Engineering and characterization of SP5.2-conjugated nanoparticles. A, Schematic diagram outlining the fabrication of SP5.2-DTX-NP using the emulsion/solvent evaporation method and N-terminal PEGylation technique. B, TEM of SP5.2-DTX-NP. C, XPS assay of copolymer mixture of aldehyde-PEG-PLA:MPEG-PLA (1:9, w/w), NP, and SP5.2-NP. Nitrogen (0.4%) was only detected in the sample of SP5.2-NP.

the recovery of the damaged tumor vasculature [6]. Multiple studies have demonstrated that such low dose metronomic chemotherapy (LDM) is superior to the MTD regimens with respect to toxicity (myelosuppression, hair loss, and nausea or vomiting, etc.) and/or survival [6].

Current metronomic chemotherapy mainly focuses on free small-molecule drugs [8,9], without any effort to achieve tumor-specific biodistribution. Such non-specific distribution may lead to long-term toxicity concerns, which should be taken into account when using metronomic chemotherapy for an extended period of time. The off-target effects of metronomic chemotherapy on the inhibition of physiological angiogenesis may affect the growth and development of young children [7]. Moreover, prolonged metronomic chemotherapy can lead to high accumulated doses of

anticancer agents, which may be associated with serious secondary diseases [7].

Metronomic chemotherapy through the specific delivery of chemotherapeutics to tumor vessels using nanoparticulate drug delivery systems (DDS) that can actively target tumor vascular EC, offers significant upside to reduce off-target side effects, decrease accumulated dose, and enhance the efficacy of tumor vessel targeting without compromising antitumor efficacy. However, there has been a lack of thorough experimental data describing targeted metronomic chemotherapy. Superior therapeutic efficacy was observed with EndoTAG-1 (paclitaxel cationic liposomes that can target tumor vessels) using a metronomic rather than an MTD approach. However, a single injection designed in the MTD regimen may compromise the MTD antitumor efficacy [10]. Tumor vessel-

targeted NGR-conjugated liposomes loaded with doxorubicin (NGR-SL[DXR]) has been developed [11]. However, NGR-SL[DXR] dosed in an MTD schedule resulted in an antitumor efficacy comparable to NGR-SL[DXR] administered using the metronomic approach, with respect to tumor growth inhibition and long-term survival [11]. Thus, the well-acknowledged advantages of metronomic chemotherapy have not yet been clearly established for DDS.

Here we explore this issue by using a new DDS with metronomic administration to actively target tumor neovasculature. It has been well demonstrated that some chemotherapeutics like DXR inhibit angiogenesis through direct cytotoxicity to EC [12], while others, like microtubule-targeted agents (MTA) such as Taxanes and *Vinca* alkaloids, exhibit remarkable antiangiogenic activity at much lower concentration that is not directly toxic to EC [13,14]. We hypothesized that docetaxel (DTX), a representative of MTA, may be more favorable when given in a dose-divided, metronomic modality. We developed SP5.2-conjugated nanoparticles loading DTX (SP5.2-DTX-NP) (Fig. 1A) for tumor vascular EC-targeting delivery. The targeting ligand SP5.2 is a peptide identified from a phage display peptide library, which can bind Flt-1 (VEGFR-1) over-expressed in tumor vessels with high affinity and specificity [15]. The *in vitro* and *in vivo* EC-targeting antiangiogenic activity and metronomic chemotherapy of SP5.2-DTX-NP were investigated.

2. Materials and methods

2.1. Materials, cell culture, and animals

Aldehyde poly(ethylene glycol)-poly(lactide) (aldehyde-PEG-PLA, MW 64 kDa) and MPEG-PLA (MW 61 kDa) block copolymers were synthesized by the ring opening polymerization in our lab as previously described [16]. SP5.2 peptide (NGYEIEWYSWVTHGMY) was synthesized by GL Biochem (Shanghai, China). DTX was supplied by Knowshine Pharmaceuticals (Shanghai, China). Taxotere was from Sanofi-Aventis. Coumarin 6 and Hoechst 33342 were from Sigma-Aldrich (St. Louis, MO). 1,1'-Diocadecyl-3,3',3'-tetramethyl indotricarbocyanine iodide (DiR) and CBQCA Protein Quantitation Kit were obtained from Life Technologies (Carlsbad, CA). VE-cadherin and Ki-67 antibody, and PE-Cy5-labeled goat anti-rabbit IgG were from Santa Cruz Biotechnology (Santa Cruz, CA). CD31 and TSP-1 antibody were from Abcam (Hong Kong). Double distilled water was purified using a millipore simplicity system (Millipore, Bedford, MA). All other chemicals were of analytical grade and used without further purification. Primary human umbilical vein endothelial cells (HUVEC) and M200 medium were obtained from Life Technologies (Carlsbad, CA). The cells at 3–5 passages were used in the experiments. The MDA-MB-231 human breast cancer cell line was from the American Type Culture Collection (Manassas, VA). Female BALB/c nude mice (20 ± 2 g) were provided by the Shanghai Laboratory Animal Center (Chinese Academy of Sciences). The animal experiment designed in this study was approved by the appropriate ethical committee of Shanghai Jiao Tong University School of Medicine.

2.2. Preparation of SP5.2-DTX-NP

SP5.2-DTX-NP were fabricated by emulsion and solvent evaporation method with a follow-up surface functionalization. Briefly, 6 mg DTX was dissolved in 1 ml solution of 60 mg blend of aldehyde-PEG-PLA and MPEG-PLA (1:9, w/w) in dichloromethane. Next, 3 ml of 1% (w/v) sodium cholate was slowly poured into the solution and then the mixture was sonicated at 240 W for 30 s (Scientz

Biotechnology, Ningbo, China). The O/W emulsion was further diluted in 40 ml of 0.5% (w/v) sodium cholate solution and then gently stirred overnight at room temperature by a magnetic stirrer to evaporate the organic solvent. The resulting DTX-loaded nanoparticles (DTX-NP) were collected by centrifugation (11,000 × g, 30 min, 4 °C; Sigma 3K18, Germany) and washed twice to remove the excessive emulsifier. Then, DTX-NP was incubated with SP5.2 at a 1:3 molar ratio of aldehyde to the N-terminal amine of SP5.2. The conjugation reaction was processed in PBS (pH 7.4) at room temperature for 10 h in the presence of NaCNBH₃ as a reducing reagent. The unconjugated SP5.2 was removed by centrifugation (11,000 × g, 30 min, 4 °C) and SP5.2-DTX-NP were collected. The coumarin 6 or DiR-labeled nanoparticles were prepared in the same way except that in the oil phase DTX was replaced or mixed with 0.3% (w/v) coumarin 6 or 0.2% (w/v) DiR, respectively.

2.3. Nanoparticle characterization

The particle size and zeta potential were determined by dynamic light scattering using a NiComp 380 ZLS instrument (Particle Sizing Systems, Santa Barbara, CA). The nanoparticles were negatively stained with 2% (w/v) sodium phosphotungstate and visualized using H-600 transmission electron microscopy (TEM) (Hitachi, Japan). Encapsulation efficiency (EE%) and drug loading (DL%) were determined as previously described [16]. The SP5.2 conjugation efficiency was determined by estimating the amount of nanoparticle-associated peptide using CBQCA Protein Quantitation Kit [11]. The SP5.2 density on nanoparticle surface and the average distance between neighboring PEG chains linked to SP5.2 were determined as previously described [17]. The X-ray photoelectron spectroscopy (XPS) was used to confirm the conjugation of SP5.2 on the nanoparticle surface [16].

2.4. Internalization mechanism of SP5.2-conjugated nanoparticles

For cell uptake examination, HUVEC were cultured on the VWR Micro Cover Glasses (VWR International, Radnor, PA) at a density of 5×10^4 cells/well in 24-well plates. When the cells reached about 80% confluence, the medium was replaced by 30 µg/ml coumarin 6-labeled nanoparticles (coumarin 6-labeled NP) or coumarin 6-labeled SP5.2-conjugated nanoparticles (coumarin 6-labeled SP5.2-NP) in medium for 1 h. After removing the nanoparticles and washing the wells twice with PBS, the cells were fixed by 4% glutaraldehyde for 20 min, and the cell nuclei were stained with Hoechst 33342 for 30 s. The cells were then observed under LSM-510 confocal laser scanning microscopy (Carl Zeiss AG, Oberkochen, Germany) using a FITC filter (Ex: 488 nm, Em: 520 nm).

To investigate the internalization mechanism, the uptake tests were performed under low temperature (4 °C) or in the presence of soluble SP5.2 (50-fold excess), filipin (10 µM, to inhibit caveolae-mediated endocytosis), cytochalasin D (3 µM, to inhibit macropinocytosis), nocodazole (10 µM, to inhibit microtubule-mediated endocytosis), chlorpromazine (30 µM, to inhibit clathrin-mediated endocytosis), phenylarsine oxide (30 µM, to deplete ATP), and nystatin (10 µM, an inhibitor of lipid-raft mediated endocytosis), respectively. HUVEC were incubated with the inhibitors for 30 min before the incubation with nanoparticles. The quantitation of coumarin 6 fluorescence in HUVEC was obtained using Zeiss LSM Image Examiner software (Carl Zeiss MicroImaging, Germany).

2.5. Circular dichroism spectrum of SP5.2 and molecular model of SP5.2 and Flt-1 complex

Circular dichroism (CD) spectrum of SP5.2 (30 µg/ml in 0.25 mM pH 7.4 Tris buffer) was recorded at room temperature in a J-715 CD spectropolarimeter (JASCO, Easton, MD). The peptide secondary structure was predicted using JASCO Spectra Manager software (version 1.5). The modeled SP5.2 structure was constructed through the alignment of the segments of 3GRN_A and 2D1Z_A structures and minimized using the CHARMM27 force field and the Born solvation model. Because SP5.2 can compete with VEGF for Flt-1 binding and inhibit a broad range of VEGF-induced events in cultured endothelial cells [15], it is hypothesized that the SP5.2 peptide interacts with the same group of residues of Flt-1. The complex of SP5.2 and

Table 1

The physicochemical characteristics of SP5.2-DTX-NP and DTX-NP.

Nanoparticles	Particle size (nm)		Zeta potential (mV)	EE ^c (%)	DL ^d (%)	CE ^e (%)	S ^f	D ^g (nm)
	DLS (PI) ^a	TEM ^b						
SP5.2-DTX-NP	175.07 ± 6.10 (0.183)	125.35 ± 5.87	-20.88 ± 1.48	41.75 ± 6.72	8.15 ± 1.21	16.14 ± 2.83	1660 ± 499	6.6 ± 0.1
DTX-NP	166.93 ± 9.98 (0.259)	113.54 ± 8.23	-24.57 ± 1.72	54.94 ± 1.46	10.53 ± 0.25	—	—	—

^a Mean hydrodynamic diameter determined by DLS. PI: polydispersity index.

^b Particle size measured by TEM.

^c Encapsulation efficiency.

^d Drug loading.

^e Conjugation efficiency.

^f SP5.2 surface density.

^g Mean distance between neighboring PEG chains which linked to SP5.2 peptide.

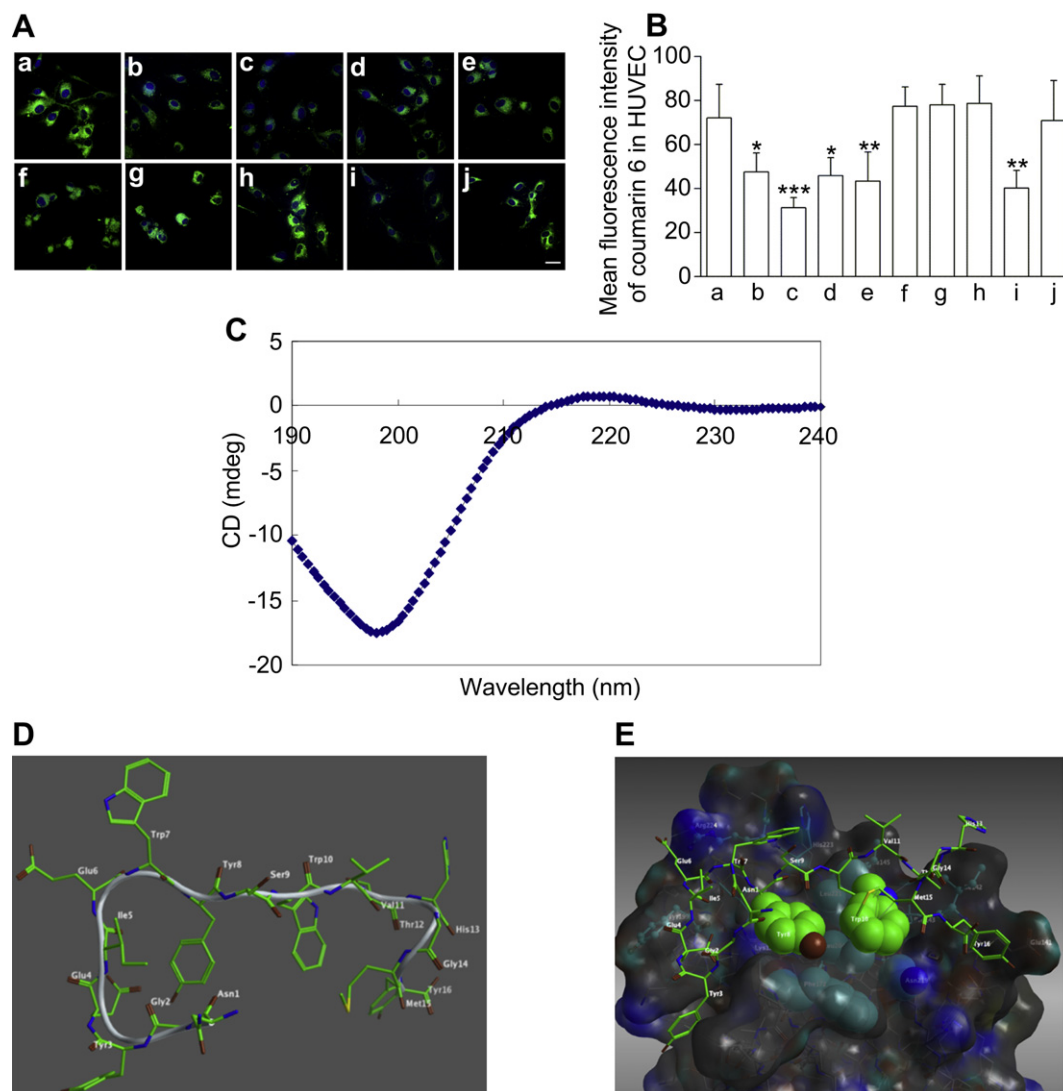


Fig. 2. SP5.2 conjugation mediates active uptake of nanoparticles into HUVEC and molecular models of SP5.2, Flt-1 domain 2, and their complex. **A**, Representative confocal laser scanning micrographs of HUVEC after 2 h incubation with coumarin 6-labeled SP5.2-NP (**a**), coumarin 6-labeled NP (**b**), or coumarin 6-labeled SP5.2-NP at 4 °C (**c**), or pre-incubated with 0.3 µg/ml free SP5.2 peptide (**d**), 10 µM filipin (**e**), 3 µM cytochalasin D (**f**), 10 µM nocodazole (**g**), 30 µM chlorpromazine (**h**), 30 µM phenylarsine oxide (**i**), 10 µM nystatin (**j**) for 30 min before the cells were exposed to coumarin 6-labeled SP5.2-NP for 2 h at 37 °C. The green presents the nanoparticles inside the cells and the blue shows the cell nuclei. Bar, 20 µm. **B**, Mean fluorescence intensity of coumarin 6 in HUVEC. Values are expressed as mean ± SD, $n = 6-8$. * $P < 0.05$, ** $P < 0.01$, *** $P < 0.001$ as compared with coumarin 6-labeled SP5.2-NP at 37 °C. **C**, CD spectrum of SP5.2 (30 µg/ml) was recorded at room temperature in 0.25 M Tris (pH 7.4), indicating the peptide exists as a random coil. **D**, Homology-modeled structure of SP5.2. **E**, The predicted binding interactions between SP5.2 and Flt-1 domain 2: H-bond interactions between Glu4 and Glu6 of SP5.2 and Lys171 and Arg224 of Flt-1, cation- π interaction between Tyr8 of SP5.2 and Lys171 of Flt-1, and most buried hydrophobic interactions of Tyr8 and Trp10 of SP5.2 with Phe172, Leu204, Asn219 and Leu221 of Flt-1. (For interpretation of the references to color in this figure legend, the reader is referred to the web version of this article.)

Flt-1 was modeled using the FlexPepDock server that enables a high-resolution protocol for modeling specific peptide-protein interaction of interest [18].

2.6. Assay of HUVEC viability, migration, and tube formation

HUVEC viability, migration, and tube formation after treatment by various DTX formulations with drug concentrations of 0.1 µM–10 nM were assayed as previously described [16]. HUVEC viabilities after 48 h treatment were determined using the Cell Counting Kit-8 (Dojindo Laboratories, Kumamoto, Japan). For metronomic treatment, HUVEC (1×10^3 cells/well) were continuously treated for 6 day, during which the medium containing the drug was changed every 24 h [9]. The cytotoxicity of various DTX formulations to MDA-MB-231 cells was also examined as control. HUVEC migration assay was performed after 8 h treatment in 24-well Transwell Boyden chambers with polycarbonate filter of 8 µm pore size (Corning, Tewksbury, MA). HUVEC tube formation after 10 h treatment was evaluated using the Chemicon *In Vitro* Angiogenesis Assay Kit (Merck Millipore, Billerica, MA). Blank NP and SP5.2-NP with the same concentrations were also examined in all cases with nanoparticles involved.

2.7. *In vivo* tumor tissue and tumor vessel targeting of SP5.2-conjugated NP

For tumor targeting study, the real-time distribution and tumor accumulation of DiR-labeled SP5.2-NP in BALB/c mice bearing MDA-MB-231 xenografts (~ 250 mm³) were monitored under the Xenogen IVIS 200 (Caliper Life Sciences, MA) noninvasive optical imaging system. The mice were injected through the caudal vein with 0.2 mg/kg of DiR-labeled NP and SP5.2-NP, respectively. After 2.5, 5.5, 24, 48, 72, and 96 h, respectively, the mice were anesthetized and imaged with an excitation bandpass filter at 710 nm and an emission at 780 nm. The exposure time for each image was 5 s. After the last animal imaging, the mice were sacrificed and tumors and other major organs and tissues (heart, liver, spleen, lung, kidney, brain, muscle, small intestine, and stomach) were harvested and placed in 24-well plate for *ex vivo* imaging. The blocking effect of 50-fold molar excess SP5.2 on the tumor tissue targeting was also evaluated.

For tumor vessel targeting test, the mice bearing MDA-MB-231 tumor (~ 250 mm³) were injected via the caudal vein with coumarin 6-labeled SP5.2-DTX-NP at DTX dose of 4 mg/kg. After 48 h, the tumors were removed and processed for cryostat sections (10 µm). The tumor vessels were stained with VE-cadherin

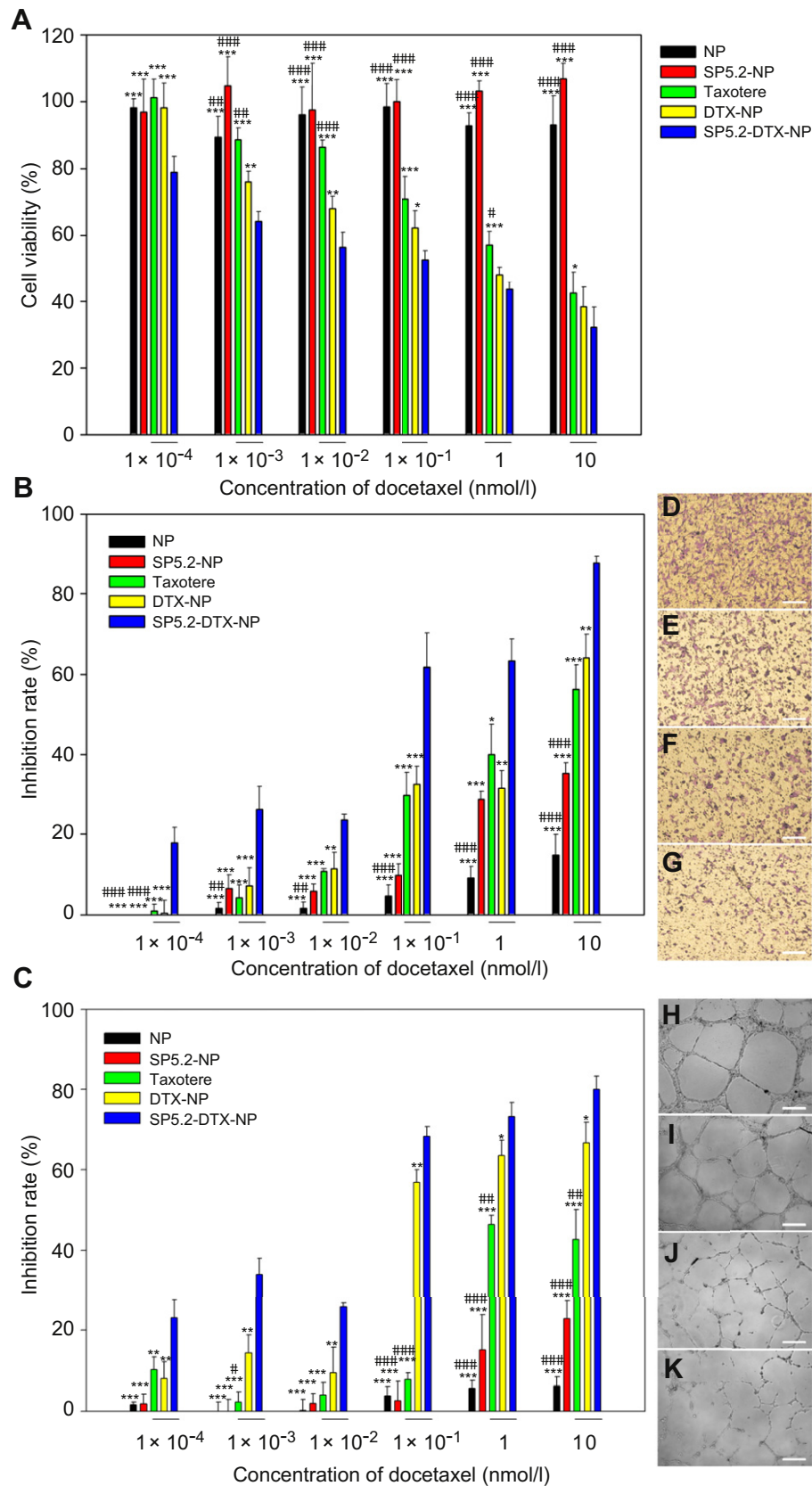


Fig. 3. SP5.2 conjugation improves nanoparticles' activity in inhibiting HUVEC proliferation, migration, and tube formation. A, Cell viability was evaluated after 48 h treatment. B, HUVEC migration after 8 h treatment was assayed using the Transwell Boyden chamber. The migrated cells were visualized by staining with crystal violet, and quantified using colorimetry after extracting the dye with acetic acid. C, Tube formation after 10 h treatment was examined using Chemicon *In Vitro* Angiogenesis Assay Kit. The representative photographs of HUVEC migration (D–G) and tube formation (H–K) after treatment with various DTX formulations at 0.1 nm were shown. D, H: control; E, I: Taxotere; F, J: DTX-NP; G, K: SP5.2-DTX-NP. Bar, 300 μ m. For blank NP and SP5.2-NP, the nanoparticle concentration was adjusted to be the same in all cases with nanoparticles involved. Values are expressed as mean \pm SD, $n = 6$. * $P < 0.05$, ** $P < 0.01$, *** $P < 0.001$ as compared with SP5.2-DTX-NP, and # $P < 0.05$, ## $P < 0.01$, ### $P < 0.001$ as compared with DTX-NP.

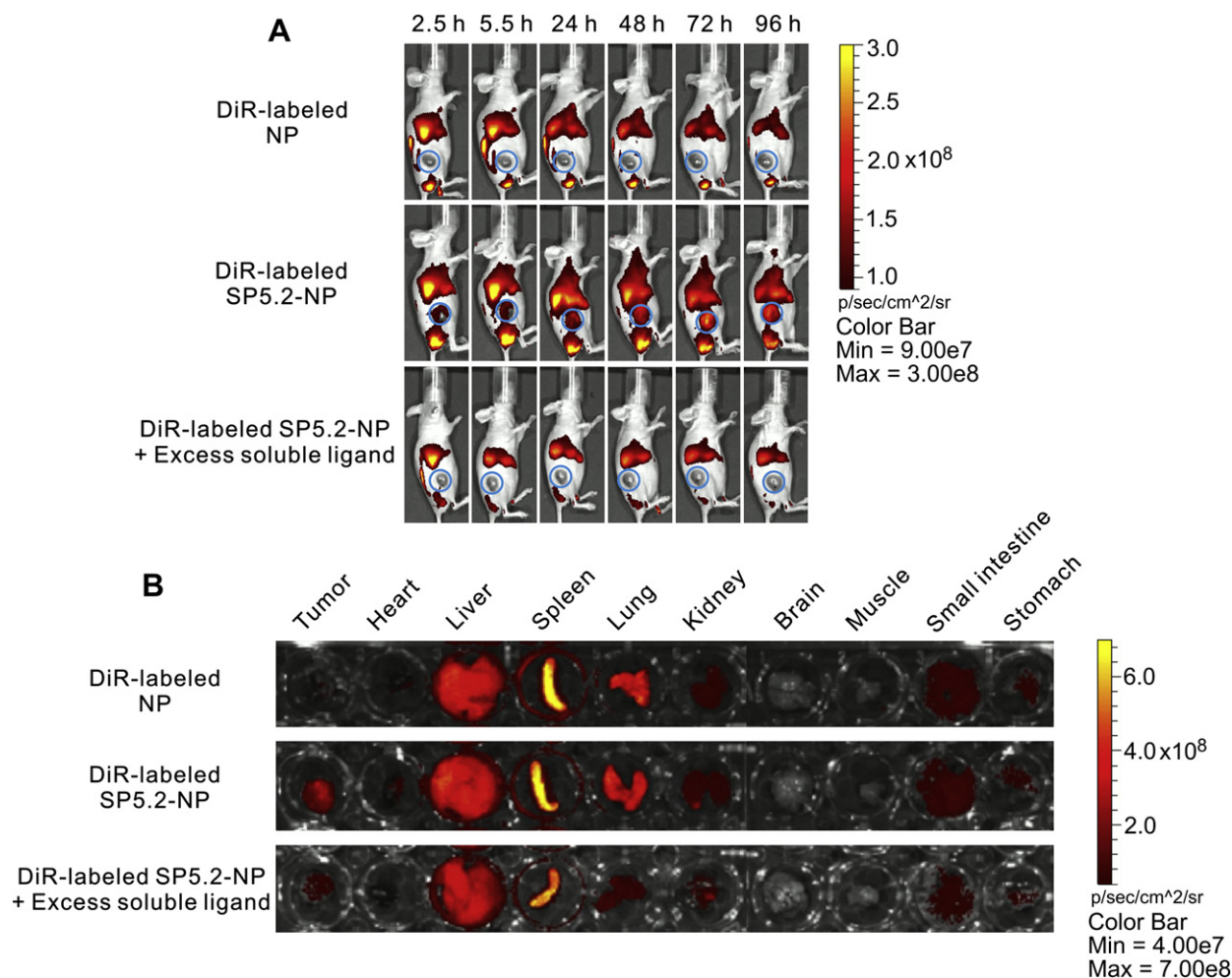


Fig. 4. SP5.2 conjugation facilitates nanoparticle accumulation in tumors. A, Female BALB/c mice bearing MDA-MB-231 tumor (~250 mm³) were given a single intravenous injection of DiR-labeled NP or SP5.2-NP at DiR dose of 0.2 mg/kg, or co-injection of DiR-labeled SP5.2-NP and excess free SP5.2. At 2.5, 5.5, 24, 48, 72, and 96 h after injection, mice with *in vivo* DiR fluorescence were imaged in Xenogen IVIS 200 system. The tumor location was indicated with blue circles. B, At 96 h after injection, the mice were sacrificed, and tumors and major organs and tissues were harvested and placed in the 24-well plate for *ex vivo* imaging. (For interpretation of the references to color in this figure legend, the reader is referred to the web version of this article.)

antibody and PE-Cy5-labeled goat anti-rabbit IgG. The apoptosis of tumor vascular EC was identified using ApopTag Red *In Situ* Apoptosis Detection Kit (Merck Millipore, Billerica, MA). The slides were observed under CLSM for VE-cadherin (PE-Cy5, Ex: 543 nm, Em: LP 650 nm), apoptosis (rhodamine; Ex: 543 nm, Em: BP 565–615 nm), and coumarin 6 (Ex: 488 nm, Em: BP 505–550 nm). The tumor paraffin sections (4 μm) were also processed for hematoxylin and eosin staining and histological examination. The blocking effect of 50-fold molar excess SP5.2 on the tumor vessel targeting was also evaluated.

2.8. Antitumor therapy of metronomic SP5.2-DTX-NP

In vivo antitumor study involved seven groups: (1) Control (saline) ($n = 6$); (2) 16 mg/kg Taxotere once weekly ($n = 6$), (3) 16 mg/kg SP5.2-DTX-NP once weekly (SP5.2-DTX-NP MTD) ($n = 6$), (4) blank SP5.2-NP with the same nanoparticle concentration in SP5.2-DTX-NP MTD once weekly ($n = 6$), (5) 3.2 mg/kg Taxotere every other day ($n = 6$), (6) Low dose metronomic 3.2 mg/kg SP5.2-DTX-NP every other day (SP5.2-DTX-NP LDM) ($n = 5$), and (7) blank SP5.2-NP with the same nanoparticle concentration in SP5.2-DTX-NP LDM every other day ($n = 6$). The study began at day 11 after tumor inoculation. Three doses (day 11, 18, and 25) for MTD (16 mg/kg) and ten doses (day 11, 13, 15, 17, 19, 21, 23, 25, 27, and 29) for metronomic therapy (3.2 mg/kg) were administered through the caudal vein to the mice, respectively. The tumor sizes were measured using calipers every other day and the tumor volumes were calculated using the formula: Volume (mm³) = (length × width²)/2. Survival observation of the mice ceased when the tumor volume reached above the ethical limit (2000 mm³) [19] or death occurred due to the toxicity after treatment. The mice body weight and daily feed and water intake were recorded throughout the study.

In a separate study, at day 30, three mice from each group were sacrificed and the tumor tissues were removed and processed for paraffin sections. The tumor

vessels and TSP-1 expression were stained using CD31 and TSP-1 antibody, respectively. Tumor cell apoptosis and proliferation were identified using ApopTag Peroxidase *In Situ* Apoptosis Detection Kit (Merck Millipore, Billerica, MA) and Ki-67 antibody, respectively. All the microphotographs were taken by Leica DFC 320 photomicroscope. The microvessel density (MVD), area percentage of TSP-1 expression, and percentage of TUNEL or Ki-67-positive cells were analyzed using Image-Pro Plus 6.0 software (Media Cybernetics, Bethesda, MD).

2.9. Toxicity evaluation

For the evaluation of DTX-associated toxicity (hematologic toxicity, bone marrow suppression, and mucosal injury), one dose (day 11) for MTD (16 mg/kg) and five doses (day 11, 13, 15, 17, 19) for metronomic therapy (3.2 mg/kg) were administered, respectively, to the mice to keep the same amount of drug exposure between MTD and metronomic treatment. Five mice from control group at day 11 and five mice from each group at day 15 and 20 were killed and blood samples were analyzed in the Advia 2120i Hematology Systems (Siemens Healthcare Diagnostics, Deerfield, IL). The marrow cells from the two femurs of each mouse were counted using a hemocytometer. The small intestines of the mice were removed, sectioned, and stained with hematoxylin and eosin for pathological assay of the villus and crypt length [20].

2.10. Statistical analysis

Statistical analysis was conducted using GraphPad Prism 5.0 software (La Jolla, CA). Differences between groups were examined using Student's *t*-test or ANOVA with Bonferroni's multiple comparison tests. Overall survival was estimated

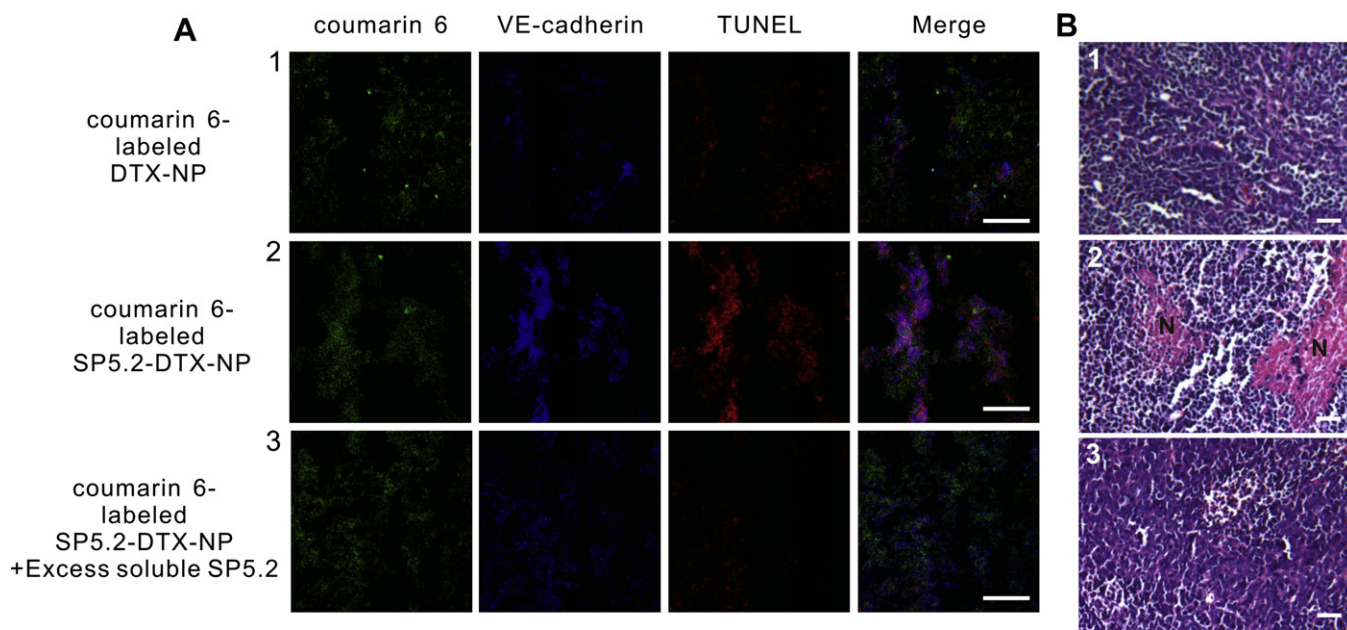


Fig. 5. SP5.2 conjugation achieves nanoparticle targeting to tumor vessel. A, Female BALB/c mice bearing MDA-MB-231 tumor ($\sim 250 \text{ mm}^3$) were intravenously administered with coumarin 6-labeled DTX-NP or SP5.2-DTX-NP at DTX dose of 4 mg/kg, or coumarin 6-labeled SP5.2-DTX-NP plus excess free SP5.2. After 48 h, the mice were killed, and the tumors were resected, sectioned, and stained for VE-cadherin (endothelial cells) (blue, pseudocolor) and TUNEL (apoptosis, red). Bar, 50 μm . The tumors were also processed for hematoxylin and eosin staining and pathological analysis (B). N, Necrosis tissues. Bar, 25 μm . Compared with coumarin 6-labeled DTX-NP (A1, B1), delivery of DTX by coumarin 6-labeled SP5.2-DTX-NP to tumor neovasculature induced significant apoptosis of endothelial cells and necrosis of tumor tissues (A2, B2), and this phenomenon can be effectively hindered by 50-fold molar excess SP5.2 peptides (A3, B3). (For interpretation of the references to color in this figure legend, the reader is referred to the web version of this article.)

according to the Kaplan–Meier method and compared using the log-rank test. Differences were considered significant if P value was less than 0.05.

3. Results

3.1. Characteristics of SP5.2-DTX-NP

The representative TEM showed that SP5.2-DTX-NP were spherical in shape with a smooth surface (Fig. 1B). The physico-chemical characteristics of the nanoparticles were summarized in Table 1. The difference between SP5.2-DTX-NP and DTX-NP in encapsulation efficiency and drug loading was not remarkable, suggesting that no significant amount of DTX leaked during SP5.2 conjugation. SP5.2-DTX-NP had an average of 1660 peptides on surface, and the mean distance between neighboring PEG chains linked to the peptide was 6.6 nm, exhibiting a multivalent ligand decoration. XPS assay showed that the surface nitrogen was only detected in the sample of SP5.2-NP with a value of 0.4% with regard to the total amount of C, O, and N atoms (Fig. 1C), indicating the successful conjugation of SP5.2 to the nanoparticle surface.

3.2. SP5.2 conjugation mediates active nanoparticle internalization in HUVEC

Compared with non-conjugated nanoparticles (coumarin 6-labeled NP), SP5.2-conjugated nanoparticles (coumarin 6-labeled SP5.2-NP) had greater intracellular accumulation that could be dramatically inhibited by excess free SP5.2, suggesting the enhanced uptake resulted from the specific interaction between SP5.2 and Flt-1 over-expressed on the endothelial cells (Fig. 2A, B).

The internalization of coumarin 6-labeled SP5.2-NP into HUVEC can also be significantly inhibited at 4 °C or in the presence of phenylarsine oxide and filipin, indicating that ATP and caveolae were involved in the uptake process. Cytochalasin D, nocodazole, chlorpromazine, and nystatin did not attenuate the uptake,

suggesting that macropinocytosis, microtubule, clathrin, and lipid-raft were not involved in the endocytosis process (Fig. 2A, B).

3.3. Molecular models of SP5.2, Flt-1 domain 2, and their complex

The homology modeling and docking test were performed to better understand the binding interaction of SP5.2 to Flt-1 at a molecular level. It has been revealed that VEGF dimmers bind to Flt-1 domain 2 through the predominantly hydrophobic interactions [21]. The surface of the important residues of Flt-1 domain 2 predicted to engage in VEGF interactions are shown in Supplementary Fig. 1A. Since SP5.2 could compete with VEGF for Flt-1 binding and inhibited a broad range of VEGF-induced events in cultured endothelial cells [15], it is hypothesized that the SP5.2 peptide interacts with the same group of residues of Flt-1. The modeled SP5.2 structure (Fig. 2D) was constructed through the alignment of the segments of 3GRN_A and 2D1Z_A structures (Supplementary Fig. 1B) and minimized using the CHARMM27 force field and the Born solvation model, showing that SP5.2 appears as an unstructured loop, which is consistent with the experimental CD spectrum (Fig. 2C). Utilizing the FlexPepDock server [18], the homology-modeled structure of SP5.2 peptide was docked to the hypothesized binding region of Flt-1 domain 2 (Supplementary Fig. 1C, D). The predicted important interactions of the SP5.2 and Flt-1 complex (Fig. 2E) were consistent with the finding from an alanine scan experiment on VEGF [22], and indicated that X residues in the SP5.2 sequence NXXEIEIXYXWXXXXXY are not directly involved in the Flt-1 binding.

3.4. SP5.2 conjugation improves nanoparticles' activity in inhibiting HUVEC proliferation, migration, and tube formation

SP5.2-DTX-NP induced significantly higher cytotoxicity to HUVEC than Taxotere at concentrations from 0.1 μM to 1 nM and than DTX-NP

at concentrations from 0.1 μM to 0.1 nM (Fig. 3A). For MDA-MB-231 cells, over 60% viability still remained after 48 h treatment by Taxotere, DTX-NP, or SP5.2-DTX-NP at even the highest drug concentration (10 nM) (data not shown). Blank NP and SP5.2-NP did not decrease HUVEC viability at all tested concentrations, indicating PEG-PLA polymer was non-cytotoxic and SP5.2 linked on the particle surface did not cause cellular toxicity to HUVEC. For metronomic 144 h treatment, the IC₅₀ value treated by SP5.2-DTX-NP for MDA-MB-231 cells was 0.083 nM , seven times higher than the level (0.012 nM) for HUVEC. These results demonstrated that relative to MDA-MB-231 cells, HUVEC were much more sensitive to SP5.2-DTX-NP.

Compared to Taxotere and DTX-NP, SP5.2-DTX-NP exhibited significantly higher activity of inhibiting HUVEC migration (Fig. 3B, D–G) and tube formation (Fig. 3C, H–K) at all tested concentrations. Although non-toxic to HUVEC, the unloaded nanoparticles and in particular, SP5.2-NP, displayed moderate ability to inhibit HUVEC migration and tube formation, indicating that SP5.2 decorated on the particle surface maintained its endogenous anti-angiogenic activity, although much less than that of model drug DTX.

3.5. SP5.2 conjugation facilitates nanoparticle distribution in tumors and achieves tumor vessel targeting

It is dramatically shown that DiR-labeled SP5.2-NP accumulated more in tumors than DiR-labeled NP only 2.5 h after injection, and this pattern maintained for the entire study (96 h after injection, Fig. 4A). *Ex vivo* imaging also confirmed that SP5.2 conjugation led to much more accumulation of nanoparticles in tumors (Fig. 4B). The tumor targeting accumulation of DiR-labeled SP5.2-NP could be efficiently blocked by free SP5.2, indicating the dominant contribution of SP5.2 to the tumor targeting of the nanoparticles.

The coumarin 6-labeled SP5.2-DTX-NP specifically targeted tumor vessels and induced apoptosis in endothelial cells, appearing as a white color merged from green (coumarin 6), blue (VE-cadherin) and red (TUNEL) (Fig. 5A2), and this also caused dramatic necrosis of tumor tissues (Fig. 5B2). In contrast, the non-specific homing to tumor neovasculature of the non-conjugated nanoparticles was very weak (Fig. 5A1, B1). The inhibition test with excessive free peptide confirmed the EC-targeting property of SP5.2-conjugated nanoparticles (Fig. 5A3, B3).

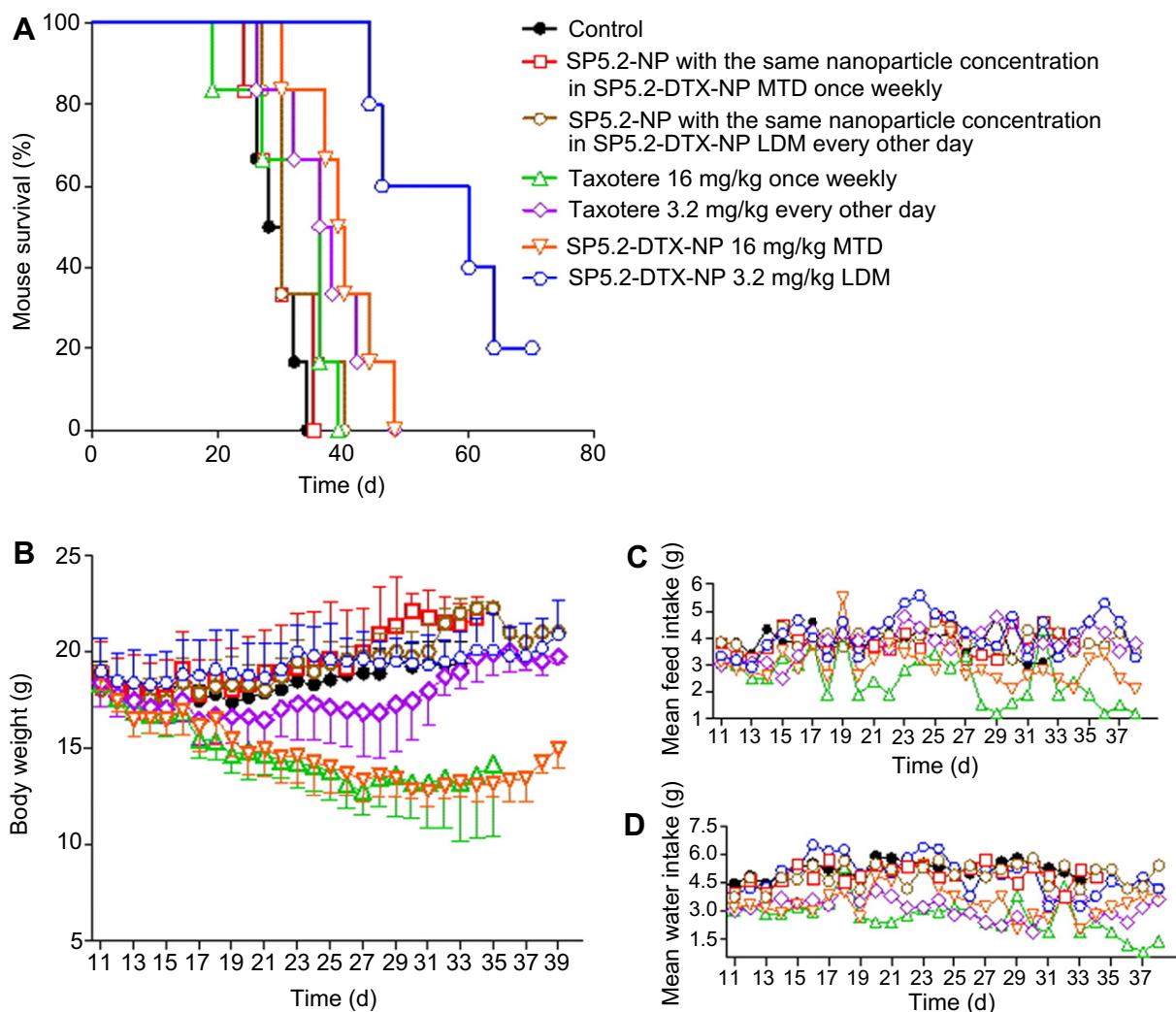


Fig. 6. Metronomic SP5.2-DTX-NP results in enhanced antitumor efficacy. Treatments to female BALB/c mice bearing MDA-MB-231 tumors started at day 11 after tumor inoculation. Ten doses (day 11, 13, 15, 17, 19, 21, 23, 25, 27, and 29) for metronomic therapy (3.2 mg/kg) and three doses (day 11, 18, and 25) for MTD (16 mg/kg) were administered through the caudal vein to the mice, respectively. Taxotere and blank SP5.2-NP given in the same regimens were also tested. A, Mice survival plot. B, Mice body weight (mean \pm SD). C, Mean feed intake. D, Mean water intake. Compared with other groups, metronomic SP5.2-DTX-NP significantly extended mice survival without accompanied toxicity to the mice, which was indicated in the well maintained body weight and feed and water uptake.

3.6. Metronomic SP5.2-DTX-NP achieves improved *in vivo* antitumor efficiency

The metronomic dose (3.2 mg/kg) was given at one day interval for total 10 injections in contrast to the 3 injections for MTD (16 mg/kg) treatment, thus the accumulative dose for metronomic therapy (32 mg/kg) was only 2/3 of that for MTD therapy (48 mg/kg). However, significantly increased medium survival was observed in the group administered with SP5.2-DTX-NP using metronomic dosing (60 days), rather than the MTD dosing (39.5 days), in which all the mice died before day 49 due to fast tumor growth and MTD treatment-associated toxicity (Fig. 6A). The blank SP5.2-conjugated nanoparticles did not have any improved antitumor effect compared to the control group. Taxotere given as 16 mg/kg once weekly or 3.2 mg/kg every other day did not produce significant antitumor efficacy due to high toxicity or rapid clearance from the blood circulation (Fig. 6, Supplementary Fig. 2).

To determine whether the improved antitumor efficacy was related to the enhanced antiangiogenic activity, immunohistochemical assays of the tumor tissues were performed. SP5.2-DTX-NP LDM resulted in significantly decreased MVD and Ki-67-positive cells, and dramatically elevated expression of TSP-1, a characteristic endogenous inhibitor of angiogenesis in metronomic chemotherapy [23,24], and TUNEL-positive cells in tumors, compared with those of other control groups (Fig. 7).

3.7. Metronomic SP5.2-DTX-NP is low toxic to the mice

The enhanced antitumor efficacy of SP5.2-DTX-NP LDM was obtained without any observable toxicity. Mice body weight in SP5.2-DTX-NP LDM group was well maintained and slightly increased at late-term of the treatment. In contrast, the mice body weight in Taxotere (16 mg/kg once weekly) and SP5.2-DTX-NP MTD

groups significantly declined by the middle and late points of the experiment (Fig. 6B). Compared with the mice in Taxotere (16 mg/kg once weekly) and SP5.2-DTX-NP MTD groups, those in SP5.2-DTX-NP LDM group had generally higher levels of daily feed and water intake (Fig. 6C, D), which reflected the better health condition of the animals and was also consistent with the superior therapeutic effect.

In a separate study, DTX-associated bone marrow suppression and hematologic toxicity were investigated (Fig. 8). The toxicities were monitored both in the medium (day 15) and the late-term (day 20) of the test. At day 15, bone marrow cells from the mice treated by Taxotere (16 mg/kg once weekly or 3.2 mg/kg every other day) decreased by 77% and 66%, respectively, compared with those of the mice in the control group, and then recovered to the normal level at day 20. However, no bone marrow suppression in the mice of SP5.2-DTX-NP LDM group appeared during the whole treatment. The white blood cells (WBC) of the mice in Taxotere (16 mg/kg once weekly) and SP5.2-DTX-NP MTD groups decreased by 46% and 41% compared with those of the mice in control group at day 15, while the WBC level did not decline in the mice of SP5.2-DTX-NP LDM group. At day 20, the WBC levels of the mice in SP5.2-DTX-NP LDM group were stable compared with those at day 11 and day 15. Other hematologic parameters such as RBC, HGB, HCT, and PLT of the mice in different treatments were all within the normal range of values, and did not vary significantly.

Mucosal injury, which leads to gastrointestinal toxicity such as nausea, vomiting, and diarrhea in clinical settings, was also examined (Fig. 9). Taxotere (16 mg/kg once weekly or 3.2 mg/kg every other day) and SP5.2-DTX-NP MTD caused significant decrease in the villus or crypt length of small intestine (jejunum) compared with the control and SP5.2-DTX-NP LDM group at day 5 and day 10. No injury to the intestine of the mice in SP5.2-DTX-NP LDM group was observed throughout the study.

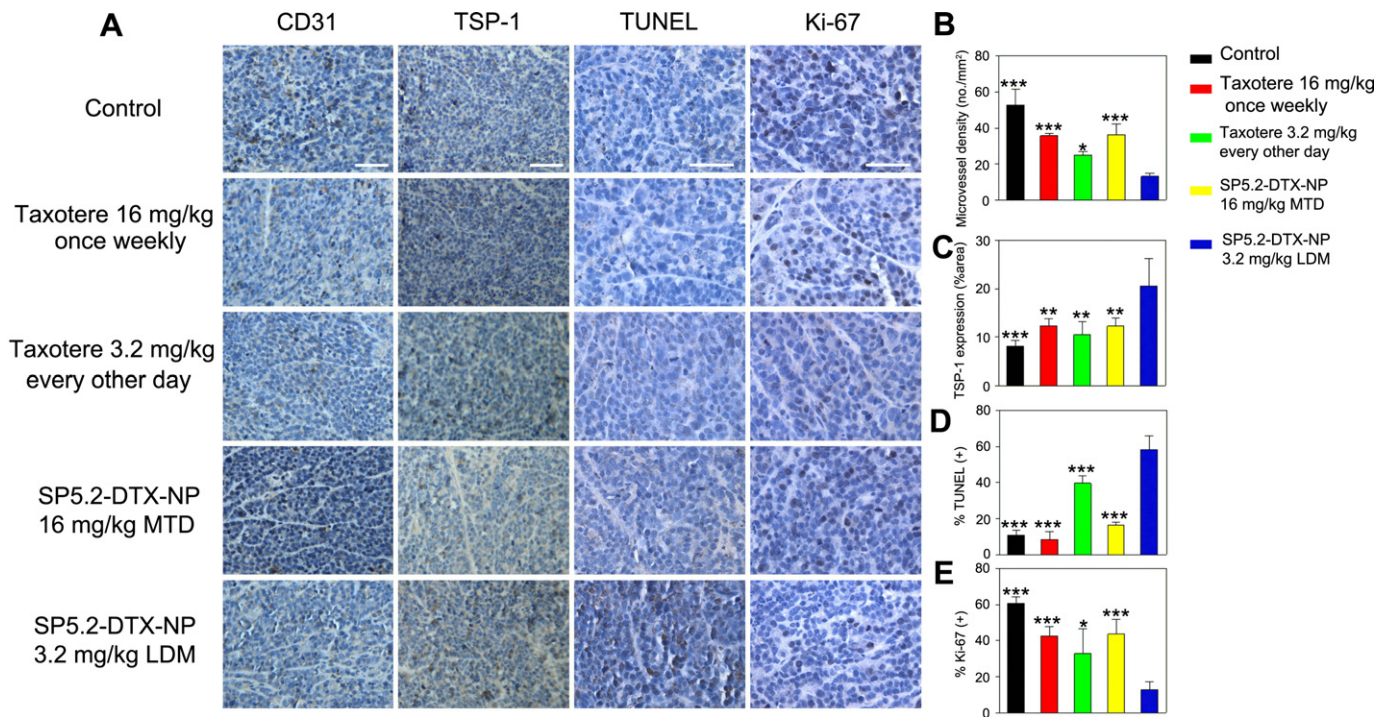


Fig. 7. Quantitative assessments of CD31 (microvessel density, MVD), TSP-1, TUNEL, and Ki-67 staining at day 30 in the therapy. A, Representative sections of CD31, TSP-1, TUNEL, and Ki-67 staining of the tumors treated by various treatments. Bar, 50 μ m. MVD (B) and percentage of Ki-67-positive proliferating cells (E) were significantly decreased, while TSP-1 expression (C) and TUNEL-positive apoptotic cells (D) are pronouncedly increased in tumors treated by SP5.2-DTX-NP 3.2 mg/kg LDM compared with other groups. Values are expressed as mean \pm SD, $n = 5$. * $P < 0.05$, ** $P < 0.01$, *** $P < 0.001$ as compared with SP5.2-DTX-NP 3.2 mg/kg LDM.

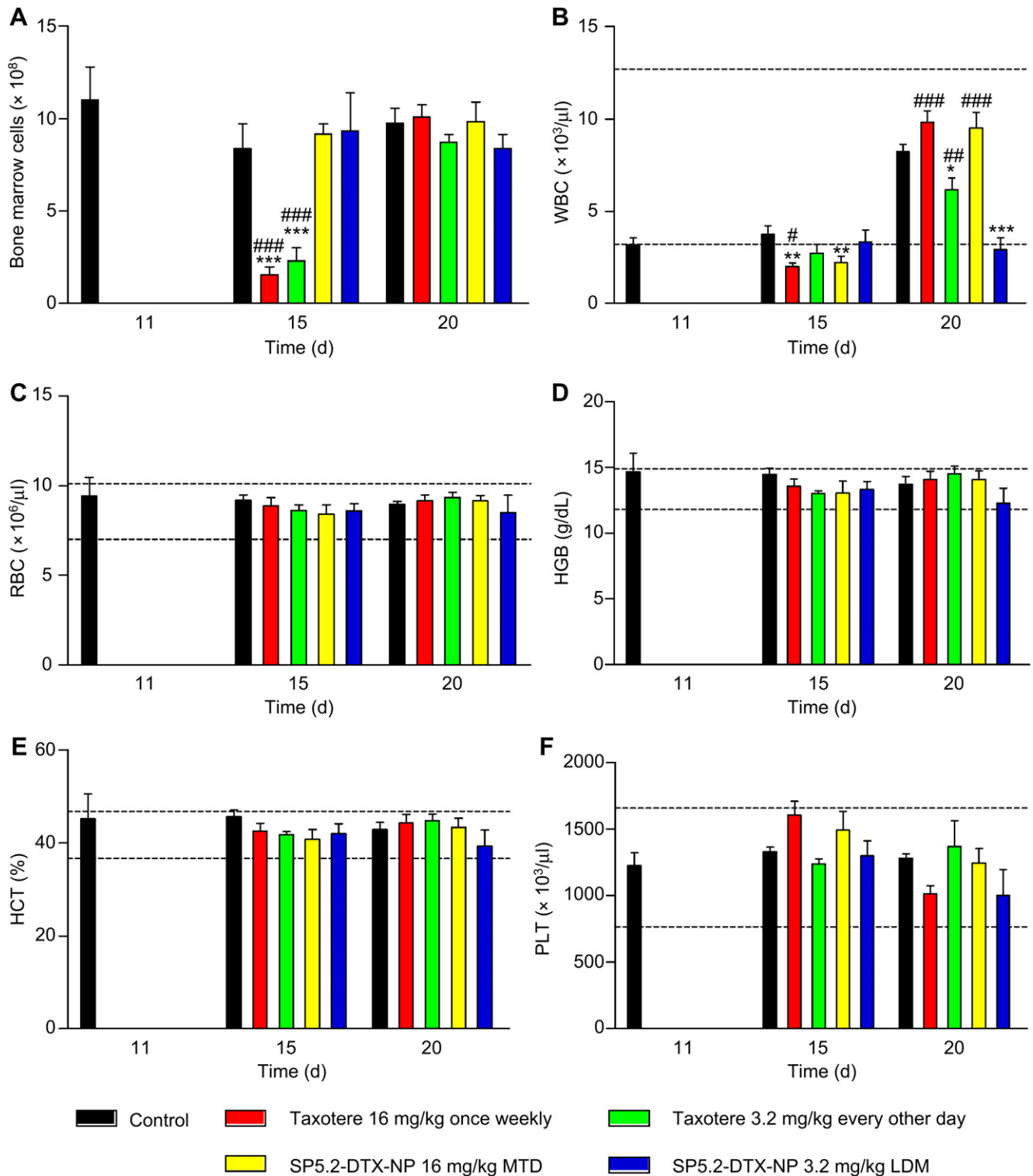


Fig. 8. Metronomic SP5.2-DTX-NP led to minimal bone marrow suppression (A) and hematologic toxicity (B–F) to the mice. Female BABL/c mice bearing MDA-MB-231 tumors were examined before (day 11) and after (day 15, 20) treatment with Taxotere or SP5.2-DTX-NP. To keep the same cumulative drug exposure between MTD and LDM treatment, one MTD dose (16 mg/kg) at day 11 and five LDM doses (3.2 mg/kg) at day 11, 13, 15, 17, and 19 were administered, respectively. The blood samples were analyzed in the Advia 2120i Hematology Systems. WBC, white blood cells; RBC, red blood cells; HGB, hemoglobin; HCT, hematocrit; PLT, platelets. The dotted lines indicate the normal range. Values are expressed as mean \pm SD, $n = 5$. * $P < 0.05$, ** $P < 0.01$, *** $P < 0.001$ as compared with control, and # $P < 0.05$, ## $P < 0.01$, ### $P < 0.001$ as compared with SP5.2-DTX-NP LDM at each day tested.

4. Discussion

To our knowledge, this is the first true example of metronomic chemotherapy using targeted nanoparticle DDS. For this

purpose, we developed SP5.2-DTX-NP. After O/W emulsion and solvent evaporation, the aldehyde groups of the polymer protruded out of the nanoparticle surface (Fig. 1A). SP5.2 was then conjugated to the aldehyde groups via its α -amino group in the presence of

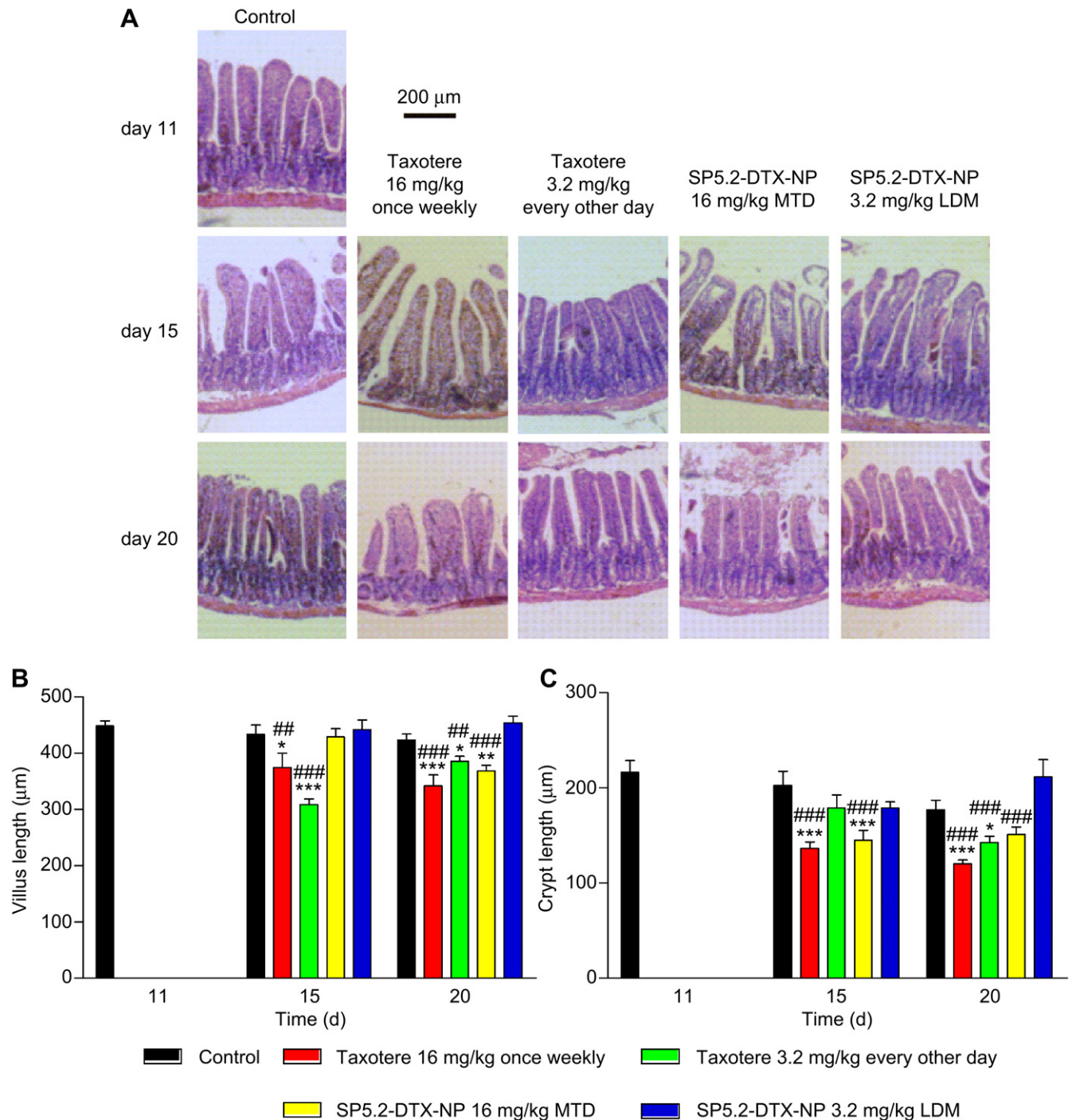


Fig. 9. Metronomic SP5.2-DTX-NP caused no mucosal injury to the mice. Female BALB/c mice bearing MDA-MB-231 tumors were examined before (day 11) and after (day 15, 20) treatment with Taxotere or SP5.2-DTX-NP. To keep the same cumulative drug exposure between MTD and LDM treatment, one MTD dose (16 mg/kg) at day 11 and five LDM doses (3.2 mg/kg) at day 11, 13, 15, 17, and 19 were administered, respectively. The small intestines of the mice were removed, sectioned, and stained with hematoxylin and eosin for pathological assay of the villus and crypt length. Values are expressed as mean \pm SD, $n = 5$. * $P < 0.05$, ** $P < 0.01$, *** $P < 0.001$ as compared with control, and # $P < 0.05$, ## $P < 0.01$, ### $P < 0.001$ as compared with SP5.2-DTX-NP LDM at each day tested.

NaCNBH₃ to generate SP5.2-DTX-NP (Fig. 1A). In this process, we utilized the technique of N-terminal PEGylation, a method that has been successfully used in one commercial product-Neulasta, a drug to treat granulocyte depletion during chemotherapy [25]. This selective N-terminal attachment of a functional ligand to the PEG chain can achieve discrete, single-positioned PEGylation and can usually preserve the conformation and biological activity of the protein or peptide [16].

The successful modification of SP5.2 was confirmed using the XPS assay of the nitrogen composition on the nanoparticle surface. An average of 1660 SP5.2 peptides were conjugated on each nanoparticle and this multivalent conjugation contributes to significantly increased, Flt-1 mediated nanoparticle internalization in HUVEC compared with the non-conjugated nanoparticles (Fig. 2A, B). Flt-1 receptor may behave differently in different conditions. Pigment epithelium-derived factor can promote the γ -secretase

mediated cleavage of Flt-1 in endothelial cells with the release of its intracellular domain fragment into the cytosol [26]; but VEGF can induce the endocytosis, a process that is probably involved with clathrin, and degradation of Flt-1 [27,28]. In this study, it appears that caveolae was involved in the nanoparticle internalization mediated by SP5.2, which was indicated by the observation of filipin inhibition (Fig. 2A, B). Similarly, the binding of many other extracellular ligands (folic acid, albumin, and autocrine motility factor) to their receptors also induce endocytosis via the caveolae [29,30]. Most importantly, the uptake through caveolae-mediated endocytosis can bypass the lysosome and alleviate drug degradation, which is highly favorable for intracellular drug delivery [31].

The important interactions of SP5.2 and Flt-1 complex were predicted through homology modeling and docking test (Fig. 2C–E, Supplementary Fig. 1), indicating that only several amino residues, but not the full peptide motif, are directly involved in the Flt-1 binding. This finding may help to better understand the binding interaction of SP5.2 to Flt-1 at a molecular level and provide clues to design alternative new peptide or small molecule with higher stability, affinity and specificity to Flt-1.

SP5.2 targeting led to dramatically enhanced antiangiogenic activity of SP5.2-DTX-NP compared with DTX-NP (Figs. 3, 5 and 7). It should be noted that the inhibition of HUVEC angiogenesis by various DTX formulations was not from the direct cytotoxicity of DTX, because at the given drug concentrations and exposure time, HUVEC proliferation was not influenced (data not shown). Compared to other kinds of chemotherapeutics such as DXR, the capability to inhibit angiogenesis far below the cytotoxic concentration to EC and tumor cells is a prominent virtue of microtubule-targeting agents [12–14], which is more favorable for low dose metronomic chemotherapy. SP5.2 conjugation significantly increased the nanoparticle distribution in tumors, which was proved in both *in vivo* and *ex vivo* imaging study (Fig. 4A, B). Although Flt-1 receptors are expressed externally in some tumor cells, MDA-MB-231 cells have Flt-1 receptors that are predominantly expressed internally and located as one of the intracellular isoforms transcribed from intron 21 (i21VEGFR-1) in the cytosol [32]. Thus, it was the targeting of SP5.2-conjugated nanoparticles to tumor EC, not MDA-MB-231 cells that led to the increased accumulation in tumors. Accordingly, the significant apoptosis of tumor EC and necrosis of tumor tissues were observed after treatment by SP5.2-DTX-NP, not DTX-NP (Fig. 5).

The optimal metronomic dose of SP5.2-DTX-NP was determined based on the MTD estimated by a dose-escalation experiment and the study of low dose metronomic treatments in decreasing CEPs (CD45⁺Flk-1⁺CD31⁺CD117⁺), a surrogate marker for angiogenesis [33–35] (Supplementary Fig. 3). The dose (3.2 mg/kg in this study) that can significantly decrease CEPs was determined to be the optimal metronomic dose [36,37]. The observation of mice survival, one of the most important criteria in anticancer therapy, showed SP5.2-DTX-NP LDM earned the best anticancer efficacy of extending mice survival compared to SP5.2-DTX-NP MTD (16 mg/kg once weekly), Taxotere (16 mg/kg once weekly or 3.2 mg/kg every other day), and other controls (Fig. 6A). Although SP5.2 on the nanoparticle surface exhibited moderate antiangiogenic activity in HUVEC (Fig. 3), its direct contribution to delay tumor growth *in vivo* was minimal (Fig. 6A) and the main role of the peptide was proved to be as a targeting agent to enable nanoparticle internalization (Fig. 2A, B). The improved antitumor efficacy of SP5.2-DTX-NP LDM was found to be well related to the enhanced antiangiogenic activity. The immunohistochemical assay revealed the remarkably decreased MVD and elevated TSP-1 expression in tumors treated by SP5.2-DTX-NP LDM compared to those of other controls (Fig. 7).

Moreover, the enhanced antitumor efficacy of SP5.2-DTX-NP LDM was obtained without any accompanied toxicity. SP5.2-DTX-

NP LDM did not lead to mice weight loss and anorexia (decreased intake of feed and water); moreover, such treatment did not lead to bone marrow suppression, hematological toxicity, and mucosal injury to the mice (Figs. 8 and 9). On the contrary, various degrees of toxicities appeared in the mice of other control groups.

5. Conclusion

Using SP5.2-DTX-NP as a model, the present study demonstrated the superior antitumor efficacy of targeted metronomic chemotherapy, which was shown in significantly prolonged survival and minimal toxicity. The distinguishing feature of our study is that we reveal and highlight the significance of targeted metronomic therapy with nanoparticulate DDS and this new modality of metronomic therapy warrants further investigation in anti-angiogenic cancer therapy.

Acknowledgments

This work was supported by National Basic Research Program of China (No. 2010CB529806), National Natural Science Foundation of China (No. 30873179, No. 81272569), Shanghai Rising-Star Program (No. 09QA1403500), Shanghai Pujiang Program (No. 12PJJD023), Shanghai Municipal Science and Technology Commission (No. 11ZR1419900, No. 11430702200), Innovation Program of Shanghai Municipal Education Commission (No. 11YZ53, No. 12ZZ200, No. 13ZZ087), Shanghai Municipal Health Bureau, and “Chen Guang” project supported by Shanghai Municipal Education Commission and Shanghai Education Development Foundation (No. 10CGB03).

Appendix A. Supplementary data

Supplementary data related to this article can be found at <http://dx.doi.org/10.1016/j.biomaterials.2013.02.017>.

References

- [1] Kerbel RS. Tumor angiogenesis. *N Engl J Med* 2008;358:2039–49.
- [2] Weis SM, Cheresh DA. Tumor angiogenesis: molecular pathways and therapeutic targets. *Nat Med* 2011;17:1359–70.
- [3] Carmeliet P, Jain RK. Molecular mechanisms and clinical applications of angiogenesis. *Nature* 2011;473:298–307.
- [4] Kluzza E, van der Schaft DW, Hautvast PA, Mulder WJ, Mayo KH, Griffioen AW, et al. Synergistic targeting of alphavbeta3 integrin and galectin-1 with heteromultivalent paramagnetic liposomes for combined MR imaging and treatment of angiogenesis. *Nano Lett* 2010;10:52–8.
- [5] Bernardes GJ, Casí G, Trüssel S, Hartmann I, Schwager K, Scheuermann J, et al. A traceless vascular-targeting antibody-drug conjugate for cancer therapy. *Angew Chem Int Ed* 2012;51:941–4.
- [6] Kerbel RS, Kamen BA. The anti-angiogenic basis of metronomic chemotherapy. *Nat Rev Cancer* 2004;4:423–36.
- [7] Pasquier E, Kavallaris M, André N. Metronomic chemotherapy: new rationale for new directions. *Nat Rev Clin Oncol* 2010;7:455–65.
- [8] Hackl C, Man S, Francia G, Milsom C, Xu P, Kerbel RS. Metronomic oral topotecan prolongs survival and reduces liver metastasis in improved preclinical orthotopic and adjuvant therapy colon cancer models. *Gut* 2013;62:259–71.
- [9] Iwamoto H, Torimura T, Nakamura T, Hashimoto O, Inoue K, Kurogi J, et al. Metronomic S-1 chemotherapy and vandetanib: an efficacious and nontoxic treatment for hepatocellular carcinoma. *Neoplasia* 2011;13:187–97.
- [10] Eichhorn ME, Ischenko I, Luedemann S, Strieth S, Pappan A, Werner A, et al. Vascular targeting by EndoTAG-1 enhances therapeutic efficacy of conventional chemotherapy in lung and pancreatic cancer. *Int J Cancer* 2010;126:235–45.
- [11] Pastorino F, Brignole C, Marimpetri D, Cilli M, Gambini C, Ribatti D, et al. Vascular damage and anti-angiogenic effects of tumor vessel-targeted liposomal chemotherapy. *Cancer Res* 2003;63:7400–9.
- [12] Hayot C, Farinelle S, De Decker R, Decaestecker C, Darro F, Kiss R, et al. *In vitro* pharmacological characterizations of the anti-angiogenic and anti-tumor cell migration properties mediated by microtubule-affecting drugs, with special emphasis on the organization of the actin cytoskeleton. *Int J Oncol* 2002;21:417–25.
- [13] Pasquier E, Honoré S, Braguer D. Microtubule-targeting agents in angiogenesis: where do we stand? *Drug Resist Update* 2006;9:74–86.

- [14] Pasquier E, André N, Braguer D. Targeting microtubules to inhibit angiogenesis and disrupt tumour vasculature: implications for cancer treatment. *Curr Cancer Drug Targets* 2007;7:566–81.
- [15] El-Mousawi M, Tchistiakova L, Yurchenko L, Pietrzynski G, Moreno M, Stanimirovic D, et al. A vascular endothelial growth factor high affinity receptor 1-specific peptide with antiangiogenic activity identified using a phage display peptide library. *J Biol Chem* 2003;278:46681–91.
- [16] Yu DH, Lu Q, Xie J, Fang C, Chen HZ. Peptide-conjugated biodegradable nanoparticles as a carrier to target paclitaxel to tumor neovasculature. *Biomaterials* 2010;31:2278–92.
- [17] Fang C, Shi B, Pei YY, Hong MH, Wu J, Chen HZ. *In vivo* tumor targeting of tumor necrosis factor- α -loaded stealth nanoparticles: effect of MePEG molecular weight and particle size. *Eur J Pharm Sci* 2006;27:27–36.
- [18] London N, Raveh B, Cohen E, Fathi G, Schueler-Furman O, Rosetta FlexPep-Dock web server-high resolution modeling of peptide-protein interactions. *Nucleic Acids Res* 2011;39:W249–53.
- [19] Upadhyay KK, Mishra AK, Chuttani K, Kaul A, Schatz C, Le Meins JF, et al. The *in vivo* behavior and antitumor activity of doxorubicin-loaded poly(γ -benzyl L-glutamate)-block-hyaluronan polymersomes in ehrlich ascites tumor-bearing BalB/c mice. *Nanomedicine* 2012;8:71–80.
- [20] Wu Z, Han X, Qin S, Zheng Q, Wang Z, Xiang D, et al. Interleukin 1 receptor antagonist reduces lethality and intestinal toxicity of 5-fluorouracil in a mouse mucositis model. *Biomed Pharmacother* 2011;65:339–44.
- [21] Wiesmann C, Fuh G, Christinger HW, Eigenbrot C, Wells JA, de Vos AM. Crystal structure at 1.7 Å resolution of VEGF in complex with domain 2 of the Flt-1 receptor. *Cell* 1997;91:695–704.
- [22] Christinger HW, Fuh G, de Vos AM, Wiesmann C. The crystal structure of placental growth factor in complex with domain 2 of vascular endothelial growth factor receptor-1. *J Biol Chem* 2004;279:10382–8.
- [23] Bocci G, Francia G, Man S, Lawler J, Kerbel RS. Thrombospondin 1, a mediator of the antiangiogenic effects of low-dose metronomic chemotherapy. *Proc Natl Acad Sci U S A* 2003;100:12917–22.
- [24] Ma J, Waxman DJ. Modulation of the antitumor activity of metronomic cyclophosphamide by the angiogenesis inhibitor axitinib. *Mol Cancer Ther* 2008;7:79–89.
- [25] Veronese FM, Pasut G. PEGylation, successful approach to drug delivery. *Drug Discov Today* 2005;10:1451–8.
- [26] Cai J, Jiang WG, Grant MB, Boulton M. Pigment epithelium-derived factor inhibits angiogenesis via regulated intracellular proteolysis of vascular endothelial growth factor receptor 1. *J Biol Chem* 2006;281:3604–13.
- [27] Kobayashi S, Sawano A, Nojima Y, Shibuya M, Maru Y. The c-Cbl/CD2AP complex regulates VEGF-induced endocytosis and degradation of Flt-1 (VEGFR-1). *FASEB J* 2004;18:929–31.
- [28] Mukherjee S, Tessema M, Wandinger-Ness A. Vesicular trafficking of tyrosine kinase receptors and associated proteins in the regulation of signaling and vascular function. *Circ Res* 2006;98:743–56.
- [29] Pelkmans L, Helenius A. Endocytosis via caveolae. *Traffic* 2002;3:311–20.
- [30] Bareford LM, Swaan PW. Endocytic mechanisms for targeted drug delivery. *Adv Drug Deliv Rev* 2007;59:748–58.
- [31] Parton RG, Simons K. The multiple faces of caveolae. *Nat Rev Mol Cell Biol* 2007;8:185–94.
- [32] Mezquita B, Mezquita J, Pau M, Mezquita C. A novel intracellular isoform of VEGFR-1 activates Src and promotes cell invasion in MDA-MB-231 breast cancer cells. *J Cell Biochem* 2010;110:732–42.
- [33] Chojiamts B, Naganuma Y, Nakajima K, Kawarabayashi T, Miyamoto S, Tachibana K, et al. Metronomic irinotecan chemotherapy combined with ultrasound irradiation for a human uterine sarcoma xenograft. *Cancer Sci* 2011;102:452–9.
- [34] Hashimoto K, Man S, Xu P, Cruz-Munoz W, Tang T, Kumar R, et al. Potent preclinical impact of metronomic low-dose oral topotecan combined with the antiangiogenic drug pazopanib for the treatment of ovarian cancer. *Mol Cancer Ther* 2010;9:996–1006.
- [35] Beaudry P, Force J, Naumov GN, Wang A, Baker CH, Ryan A, et al. Differential effects of vascular endothelial growth factor receptor-2 inhibitor ZD6474 on circulating endothelial progenitors and mature circulating endothelial cells: implications for use as a surrogate marker of antiangiogenic activity. *Clin Cancer Res* 2005;11:3514–22.
- [36] Bertolini F, Paul S, Mancuso P, Monestiroli S, Gobbi A, Shaked Y, et al. Maximum tolerable dose and low-dose metronomic chemotherapy have opposite effects on the mobilization and viability of circulating endothelial progenitor cells. *Cancer Res* 2003;63:4342–6.
- [37] Shaked Y, Emmenegger U, Man S, Cervi D, Bertolini F, Ben-David Y, et al. Optimal biologic dose of metronomic chemotherapy regimens is associated with maximum antiangiogenic activity. *Blood* 2005;106:3058–61.